

1 **Distributions and stoichiometry of dissolved nitrogen and phosphorus in the iron**
2 **fertilized region near Kerguelen (Southern Ocean).**

3

4 S. Blain^{1,2}, J. Capparos^{1,2}, A. Guéneuguès^{1,2}, I. Obernosterer^{1,2}, and L. Oriol^{1,2}

5 ¹Sorbonne Universités, UPMC Univ Paris 06, UMR7621, Laboratoire d'Océanographie

6 Microbienne, Observatoire Océanologique, 66650 Banyuls/mer, France

7 ²CNRS, UMR7621, Laboratoire d'Océanographie Microbienne, Observatoire Océanologique,

8 66650 Banyuls/mer, France

9

10 **Abstract**

11

12 During KEOPS2 (Kerguelen Ocean and Plateau Compared Study 2), we determined
13 dissolved inorganic and organic nitrogen and phosphorus species in the naturally fertilized
14 region of Kerguelen Island (Southern Ocean,). Above 150m, stations were clearly separated
15 by the Polar Front (PF), with concentrations of NO_3^- , NO_2^- and PO_4^{3-} overall lower north than
16 south of the PF. Though less pronounced, a similar trend was detectable for dissolved organic
17 nitrogen (DON) and phosphorus (DOP). At all stations offshore and above the plateau, a
18 subsurface maximum of NH_4^+ was observed between 50 and 150 m. We examined nutrient
19 stoichiometry by calculating the linear combination $\text{N}^* = [\text{NO}_3^-] - 16 [\text{PO}_4^{3-}]$. The majority of
20 stations and depths revealed N^* close to $-3 \mu\text{M}$, however, for surface waters north of the PF
21 N^* increased up to $6 \mu\text{M}$. This suggests a preferential uptake of PO_4^{3-} versus NO_3^- by fast
22 growing diatoms. Using the tracer $\text{TN}_{\text{xs}} = [\text{TDN}] - 16[\text{TDP}]$ revealed that the dissolved
23 organic fraction significantly contributed to changes in TN_{xs} . TN_{xs} were negative for most
24 stations and depths, and relatively constant in the layer 0-500m. As for N^* , the stations north

25 of the PF had higher TN_{xs} in the layer 0-100m. We discuss this stoichiometric anomaly with
26 respect to possible external sources and sinks of N and P. Additional data collected in
27 February 2013 at two sites revealed the occurrence of a subsurface minimum of N^* located
28 just below the pycnocline that denotes a layer where remineralization of particulate organic
29 matter with low N:P ratio P, possibly associated with preferential remineralisation of P versus
30 N, persists throughout the season.

31 **1. Introduction.**

32 The first scientific expeditions in the Southern Ocean discovered high concentrations of major
33 nutrients such as nitrate (NO_3^-) and phosphate (PO_4^{3-}) in surface waters south of $50^\circ S$ (Hart,
34 1942). The general meridional overturning circulation that brings deep water to the surface at
35 the southern limits of the Antarctic circumpolar current (Marshall and Speer, 2012) is the
36 major mechanism supplying surface waters with NO_3^- and PO_4^{3-} . Most of the nutrient-rich
37 upwelled waters are transported northward and they leave the surface north of the Polar Front,
38 through their transformation into intermediate and mode waters. Despite the several months
39 long northward transport during which the NO_3^- and PO_4^{3-} rich waters are exposed to sunlight,
40 little phytoplankton biomass develops. This system was characterized as “high nitrate low
41 chlorophyll” (HNLC). The major consequence of the HNLC status of the Southern Ocean is
42 that large amounts of unused nutrients are transported back into the ocean interior where they
43 feed the main thermocline and finally supply low and mid latitude surface waters with
44 essential nutrients (Sarmiento et al., 2004). Another consequence is that similarly to NO_3^- and
45 PO_4^{3-} , large amounts of upwelled dissolved inorganic carbon (DIC) are not converted to
46 particulate organic carbon (POC) and remain in contact with the atmosphere for time periods
47 long enough to degas carbon dioxide (CO_2) with important consequences for climate (Sigman
48 and Boyle, 2000).

49 The iron hypothesis (Martin and Fitzwater, 1988) was a major advancement for our
50 understanding of the HNLC paradox. More than two decades of intense research have
51 confirmed that increasing iron supply stimulates primary production, major nutrient utilization
52 and the air-to-sea flux of CO₂ in surface waters. Nutrient utilization in surface waters is
53 therefore a diagnostic of the efficiency of the biological pump of CO₂. Nitrate utilization has
54 also received much attention in paleoceanographic studies, because it can be inferred from the
55 isotopic composition of N in bulk material or specific compounds of fossil organisms
56 preserved in the sediment. Recent results provide support to the enhanced NO₃⁻ utilization
57 related to higher dust deposition during the ice ages in the sub Antarctic region (Martinez-
58 Garcia et al., 2014).

59 Early modelling studies on the iron hypothesis were conducted using models that did
60 not explicitly represented the iron cycle. The effect of iron fertilization was mimicked using
61 the extreme assumption that iron fertilization results in the complete depletion of N or P in
62 surface waters (Gnanadesikan et al., 2003; Sarmiento and Orr, 1991). However, this was never
63 observed during artificial iron fertilization (Boyd et al., 2007), iron addition during deck
64 incubations (Moore et al., 2007) or in naturally iron fertilized regions (Blain et al., 2007). For
65 most previous research in this context, it was assumed that NO₃⁻ and PO₄³⁻ behave in a similar
66 way. This is only true at first order because interesting differences were noticed (Jenkins et
67 al., 1984; Minas and Minas, 1992; Lourey and Trull, 2001). Weber and Deutsch (Weber and
68 Deutsch, 2010) used zonal mean distributions of NO₃⁻ and PO₄³⁻ in the Southern Ocean to
69 reveal that the differential utilization of both nutrients is likely related to the composition of
70 the phytoplankton community. Detailed investigations of blooms in varying regions of the
71 Southern Ocean confirm different utilization of NO₃⁻ and PO₄³⁻ depending on the dominant
72 species in the phytoplankton community (Arrigo, 1999; De Baar et al., 1997; Moore et al.,
73 2007). In addition, the possible role of DOP and DON for N and P decoupling has not been

74 investigated, although modeling studies suggest that these organic forms may significantly
75 contribute to the cycling of N and P in the Southern Ocean (Wang et al., 2003).

76 Our work presents new data on dissolved inorganic and organic nitrogen and phosphorus
77 concentrations from the iron-fertilized regions near the Kerguelen archipelago. We present
78 their spatial and temporal distributions, and discuss their stoichiometry.

79 **2. Material and methods**

80 **2.1 Sampling**

81 During KEOPS2, the samples were collected at the stations presented on the map in Fig.1.
82 The coordinates and date of sampling are summarized in suppl table 1. Additional samples
83 were collected during the cruise KEOPSMOOR in February 2013 at stations A3 and at station
84 TNS-6 (suppl table 1). The samples for dissolved nitrogen and phosphorus analyses were
85 collected with 22 12 liter Niskin bottles mounted on a rosette equipped with a Seabird
86 SBE911-plus CTD unit. In this work, we used potential temperature (θ) and density anomaly
87 (σ) to characterize the hydrology of the stations. A more complete description of the
88 hydrology and the circulation is presented in (Park et al., 2014).

89 For NO_3^- , PO_4^{3-} and nitrite (NO_2^-), syringes (50 mL) were directly connected to the spigot of
90 the Niskin bottles. The samples were drawn through a 0.45 μm Up-tidisc (Whatman) adapted
91 to the syringe. Duplicate samples were collected. The second sample (25 mL) was poisoned
92 with mercuric chloride (HgCl_2 , 20 mg L^{-1} , final concentration) and stored in the dark at room
93 temperature for later analysis. .

94 For ammonium (NH_4^+), samples were collected from Niskin bottles in two 50 mL Schott
95 glass bottles. Following rinsing, the bottles were filled with 40 mL of seawater and closed
96 immediately to avoid contamination by air. Back in the aboard laboratory the oxidative
97 reagent (Holmes et al., 1999) was added. Samples for NH_4^+ determination were incubated for

98 at least 3 hours in the dark, at ambient temperature, before fluorescence measurements
99 ($\lambda_{\text{exc}}=370 \text{ nm}$ $\lambda_{\text{emi}}=460 \text{ nm}$) with a fluorimeter (Jabsco).

100 For dissolved organic nitrogen (DON) and phosphorus (DOP) analysis the samples were
101 collected from Niskin bottles in 100 mL Schott glass bottles. The Schott glass bottles were
102 rinsed with HCl (10%) and several times with ultrapure water (prepared by deionization and
103 UV sterilization) between casts. The samples were then filtered through 2 combusted GF/F
104 filters. 20 mL of the filtered samples were transferred to 20 mL PTFE vials and poisoned with
105 100 μl of HgCl_2 (4 g L^{-1} , working solution) before storage at 4°C . All analyses were
106 performed aboard as described below.

107 **2.2 Analytical methods**

108 For NO_3^- , NO_2^- , PO_4^{3-} , one sample was immediately analyzed aboard with a
109 segmented flow analyzer (Skalar) equipped with colorimetric detection using methods
110 described in (Aminot and K erouel, 2007). The accuracy of the methods was assessed using
111 reference material (Certipur, Merck). The precisions were in the range 1-4 %, and the limit of
112 detection was $0.02 \mu\text{M}$ for NO_3^- and NO_2^- , $0.03 \mu\text{M}$ for PO_4^{3-} .

113 Samples for DON and DOP determination were spiked with 2.5 mL of the oxidative reagent
114 (boric acid + sodium hydroxide + potassium peroxodisulfate), and then heated at 120°C for 30
115 min. After cooling, the concentrations of NO_3^- and PO_4^{3-} were determined as mentioned
116 above. This provides the concentrations of Total Dissolved Nitrogen (TDN) and Total
117 Dissolved Phosphorus (TDP). The concentrations of DON and DOP were calculated as
118 follows; $\text{DON}=\text{TDN}-[\text{NO}_3^-]-[\text{NO}_2^-]$ and $\text{DOP} = \text{TDP}-[\text{PO}_4^{3-}]$.

119

120 **3. Results**

121 Most of the stations are located south of the Polar Front (PF), with the exception of the coastal
122 stations TEW-1-2 and the offshore stations TNS-1-2, TEW-7-8 and F-L that were located
123 north of the PF (Fig.1). Station R-2, located west of the plateau had low chlorophyll
124 concentrations in surface water throughout the season ($\sim 0.3 \text{ mg m}^{-3}$)(Lasbleiz et al., 2014), an
125 observation that is explained by the low iron supply (Qu  rou   et al. this issue). By contrast, all
126 other stations were characterized by the development of large spring blooms consistent with
127 higher iron supply(Lasbleiz et al., 2014). However, the development of the blooms within the
128 iron fertilized region was not homogenous in time and space. A3-1, and stations TNS-1 to
129 TNS-10 of the North-South transect, sampled at the beginning of the spring bloom, were
130 characterized by low chlorophyll concentrations only slightly higher than that at station R-2.
131 Stations TEW-1 to TEW-8 of the East-West transect, stations E-2 to E-5, and station A3-2
132 (second visit at station A3), were sampled a few days later, when the bloom rapidly developed
133 with large spatial heterogeneity. The largest stocks of chlorophyll *a* within the 0-200 m layer
134 were observed at stations F-L north of the PF and at station A3-2 above the plateau. Based on
135 the trajectories of 2 surface drifters (Zhou et al., 2014), stations E-1, E-2, E-3, E4-E and E-5,
136 are assumed to evolve in a quasi Lagrangian framework and their succession in time can be
137 considered at the first order as a time series.

138 **3.1 Two dimensional distributions of dissolved nitrogen and phosphorus.**

139 In the upper 200m of the water column, concentrations of NO_3^- and PO_4^{3-} were $\geq 19 \mu\text{M}$ and
140 $\geq 1 \mu\text{M}$, respectively (Fig. 2 and 3). Concentrations were higher west of the PF (transect EW,
141 Fig. 2) and South of the PF (transect NS, Fig. 3) and lower in surface Subantarctic waters,
142 north and east of the PF. Concentrations of NO_2^- were the highest above 150m, and below this
143 depth NO_2^- decreased rapidly to reach values close to the limit of detection at 200m. Above
144 150m, NO_2^- concentrations were clearly higher at the stations in the Polar Front zone

145 (PFZ)(NO₂⁻ in the range 0.3-0.4 μM) than at those in the Antarctic Zone (AZ)(NO₂⁻ of 0.25
146 μM).

147 Along the transect EW, the highest NO₂⁻ concentrations were measured at TEW-1 (0.31-0.34
148 μM). Contrasting with the NO₂⁻ distribution observed along the transect NS, the stations of
149 the AZ (i.e. west of the isocline sigma=27) had higher concentrations than those of the PFZ.
150 NH₄⁺ concentrations were highest at the coastal stations. At Stations TEW-1, concentrations of
151 NH₄⁺ increased from 0.19 μM (at 10m) to 1.45 μM (close to the bottom). The same trend was
152 observed at TEW-2 (0.17 μM at 10m and 0.39 μM close to the bottom). At all stations
153 offshore and above the plateau, a subsurface maximum of NH₄⁺ peaking at 0.5-0.6 μM was
154 observed between 50 and 150 m. The DON distribution was characterized by a north-south
155 gradient in the 0-150 m layer. DON concentrations above the Kerguelen plateau at Stations
156 A3-1 and TNS-10 (6.0±1.0 μM) were similar to those the meander of the PF 6.4±1.7 μM
157 (stations TNS-3 to TNS-7). But higher values were detectable north of the PF (8.6±1.2 μM for
158 stations TNS-1 and TNS-2). .

159 For DOP, the latitudinal gradient was less pronounced, but DOP concentrations were lower
160 above the Kerguelen plateau than at any other sites.

161 **3.2. Speciation of dissolved nitrogen at selected sites.**

162 **3.2.1. The Kerguelen plateau station A3**

163 The vertical distribution of different chemical nitrogen species during the two visits at station
164 A3 are detailed in figure 4. NO₃⁻ distributions are discussed in more detail in section 3.3.

165 Concentrations of NO₂⁻ were, during both visits, homogeneous in the mixed layer and
166 revealed a small maximum below the mixed layer depth (MLD). NO₂⁻ increased from 0.27
167 μM at A3-1 to 0.33 μM at A3-2 (Fig. 4b). NH₄⁺ concentrations roughly doubled between the
168 two visits (0.1 μM at A3-1 to 0.2 μM at A3-2) and clear maxima were detectable at the base

169 of the mixed layer. Concentrations of DON did not change between visits, however DON
170 accounted for 20% of TDN in the mixed layer at A3-1, and this contribution increased to 25%
171 in the upper 40 m water layer at A3-2 (data not shown). Both NO_3^- consumption and DON
172 release during the 4 weeks that separated the two visits explained the increase in the percent
173 DON of TDN. Below 200 m, TDN was higher at A3-1 than at A3-2. This was mainly driven
174 by the differences in DON concentrations that were higher at A3-1 (4.7-6.7 μM) than at A3-2
175 (1.8-4 μM) in the 250-300 m layer (Fig. 4).

176 **3.2.2. Stations F-S and F-L north of the Polar Front**

177 Distinct vertical profiles of NO_2^- and NH_4^+ were observed at station F-S. Concentrations of
178 NO_2^- decreased from 0.39 μM at 10 m to 0.22 μM at 93 m. However, we note a remarkably
179 low value of 0.15 μM at 79 m (Fig. 5a). The NH_4^+ profile presented the same anomaly,
180 resulting in two subsurface maxima. This feature contrasts with most other stations where a
181 single subsurface maximum was observed, as for example at station F-L (Fig. 5b) located a
182 few nautical miles away from F-S. We suggest that this anomaly is due to the position of F-S
183 within the Polar Front where a complex mixing event at small scale could have occurred. The
184 contribution of DON to TDN at F-S decreased continuously from 34% at 20 m to 9% at 120
185 m. However, close to the surface the contribution of DON was only 17% (Fig. 5d).

186 **3.2.3. The HNLC station R-2**

187 The vertical distribution of NO_3^- and DON revealed small variations between the surface and
188 200 m (Fig. 6a). DON accounted for 19% to 24% of TDN, representing intermediate values as
189 compared to the range observed in the fertilized region. Concentrations of NO_2^- and NH_4^+
190 presented similar vertical distributions, decreasing rapidly below the mixed layer (Fig. 6b).
191 Concentrations of NH_4^+ in the mixed layer (0.07 μM) were at least two fold lower than at any
192 other stations, and NO_2^- concentrations in the mixed layer (0.3 μM) were similar to those of
193 the mixed layers in the fertilized regions.

194 **3.2.4. Lagrangian sites E**

195 All stations were characterized by similar vertical distributions of NO_2^- and NH_4^+ .
196 Concentrations in the mixed layer were in the range 0.25-0.3 μM decreasing to 0.02-0.03 μM
197 below 200 m. The vertical distributions of NH_4^+ are characterized by a subsurface maximum
198 with concentrations (0.4-0.65 μM) two fold higher than at the surface (0.2-0.3 μM). NO_3^-
199 distributions are described in more detail in the next section. The contribution of DON to
200 TDN in the mixed layer was in the range 15-25%. No clear temporal evolution was
201 detectable.

202 **3.3. Temporal evolution of the vertical distributions of nitrate and phosphate**

203 **3.3.1. The Lagrangian sites E**

204 The vertical profiles of NO_3^- and PO_4^{3-} concentrations in the upper 200 meters of 5 stations
205 located in the center of a meander of the PF are presented in Fig. 7. In addition, we show data
206 from two other cruises. Samples collected in early October 1995 during the cruise
207 ANTARES3 (Blain et al. 2001) provided data typical of winter conditions. Samples of the
208 KEOPSMOOR profile were collected in February 2013, representing post bloom conditions.
209 Concentrations of NO_3^- were almost identical among visits at 150 m (mean $27.5 \pm 0.8 \mu\text{mol}$
210 L^{-1} , Fig. 7a). Above 150 m, NO_3^- concentrations change along the season. In winter,
211 concentrations were homogenous from surface to 150 m, resulting in a mean integrated stock
212 of $4.22 \pm 0.08 \text{ mol m}^{-2}$. In spring, the KEOPS2 profiles qualitatively clustered in two groups.
213 The first cluster is composed of stations TNS-5, TNS-6, E-1, E-2 and E-3, with higher NO_3^-
214 concentrations (mean integrated stock 0-150m of $4.10 \pm 0.05 \text{ mol m}^{-2}$) than in the group
215 formed by stations E4-E and E-5 (mean integrated stock 0-150m of $3.90 \pm 0.04 \text{ mol m}^{-2}$).
216 Finally, the lowest concentrations were measured in summer (mean integrated stock 0-150m
217 of 3.48 mol m^{-2}).

218 Vertical profiles of PO_4^{3-} presented similar characteristics as NO_3^- , with the exception of the
219 winter profile (Fig. 7b). The winter profile indicates that PO_4^{3-} concentrations are
220 homogeneously mixed in the upper 150m. The concentrations seem overestimated at 150m and
221 above. We do not think that the differences result from inter-annual variability because this
222 would have also impacted NO_3^- concentrations. The high concentrations of PO_4^{3-} measured in
223 winter 1995 lead to a $\text{NO}_3^-:\text{PO}_4^{3-}$ ratio of 12.5 which is low. The overestimation of PO_4^{3-}
224 could result from methodological issues. The ANTARES3 samples were not analyzed
225 aboard, but a few months later in a laboratory by a different analytical protocol. The lack of
226 certified international standards necessary for a strong quality control of the accuracy
227 precludes rigorous comparison of sample collected in 1995 with more recent samples.

228 Similarly to NO_3^- , we consider the mean concentration of PO_4^{3-} at 150 m (excluding the
229 ANTARES3 PO_4^{3-} value) to estimate a mean winter PO_4^{3-} concentration in the surface layer of
230 $1.93 \pm 0.09 \mu\text{mol L}^{-1}$, that yields an integrated winter stock of $0.30 \pm 0.02 \text{ mol m}^{-2}$. The
231 integrated stock for the group of stations E-1-2-3 ($0.280 \pm 0.004 \text{ mol m}^{-2}$) was higher than for
232 the group E-4-5 ($0.274 \pm 0.005 \text{ mol m}^{-2}$). At the end of the season the integrated PO_4^{3-} stock
233 was 0.250 mol m^{-2} .

234 **3.3.2. The Kerguelen plateau station A3**

235 At Station A3, vertical profiles of changes of NO_3^- and PO_4^{3-} concentrations were observed
236 between spring and summer (Fig. 8). Albeit the stations were sampled in November 2011 and
237 February 2013, we consider these variations as seasonal changes. The profiles of both
238 nutrients merge at 200 m in early spring and summer (A3-1 and A3-2). However, during the
239 second visit at A3 (A3-2), we observed that the surface layer was mixed down to 170 m. We
240 propose that the concentrations at 200 m are a good estimate of the winter concentrations of
241 NO_3^- and PO_4^{3-} at this station. Thus, winter stocks (0-200m) were 6.27 and 0.43 mol m^{-2} for
242 NO_3^- and PO_4^{3-} , respectively. At the first visit at station A3 the stocks had decreased to 5.96

243 and 0.41 mol m^{-2} . Four weeks later (A3-2) they reached 5.29 and 0.36 mol m^{-2} . Finally, in
244 February the stocks were 4.77 and 0.35 mol m^{-2} .

245 **5. Discussion.**

246 The distributions of NO_3^- and PO_4^{3-} in the world's oceans were extensively studied over the
247 past decades. A major rationale for this research is the critical role of these major nutrients for
248 phytoplankton growth and therefore marine primary production. Further, concentrations of
249 NO_3^- and PO_4^{3-} are used as tracers for biogeochemical processes in the ocean (Deutsch and
250 Weber, 2012). In the Southern Ocean, south of the Subantarctic front, NO_3^- and PO_4^{3-}
251 concentrations are high. They are therefore considered as non-limiting and much less attention
252 has been paid to their distributions if compared to other nutrients such as silicic acid or
253 dissolved iron. However, the relief of iron limitation by natural or artificial fertilizations
254 offers a different perspective because NO_3^- and PO_4^{3-} should be consumed as the bloom
255 develops. This has motivated the present detailed study of dissolved N and P in the naturally
256 fertilized region of Kerguelen.

257 To explore the dynamics of NO_3^- and PO_4^{3-} we examined their stoichiometry in the
258 study region. This is commonly done by establishing the ratio $r_{\text{N:P}} = [\text{NO}_3^-] : [\text{PO}_4^{3-}]$ for
259 comparison with the Redfield ratio of 16 (Redfield et al., 1963). However, the interest of $r_{\text{N:P}}$
260 is limited because this ratio is not conserved by mixing or biological processes such as uptake
261 or remineralisation (Deutsch and Weber, 2012). We therefore calculated the linear
262 combination $\text{N}^* = [\text{NO}_3^-] - 16 [\text{PO}_4^{3-}]$, similar to the parameter first introduced by (Michaels et
263 al., 1996), but omitting the constant term required to obtain a global average of N^* equal to 0.
264 N^* traces the impact of processes that add or remove N and P with a stoichiometry different
265 from the Redfield ratio of 16. At almost all stations and depths, N^* was close to $-3 \mu\text{M}$ (Fig.
266 9a). This value agrees well with the mean N^* computed for regions of the Southern Ocean

267 close to the PF (Weber and Deutsch, 2010). A noticeable deviation from this value was
268 observed for a set of data where N^* increased from $N^*=-3 \mu\text{M}$ to $N^*=6 \mu\text{M}$. All data with
269 $N^*>0$ are for samples collected in the mixed layer north of the PF, and located in a bloom
270 where diatoms contributed 70 % of the carbon biomass in the euphotic layer(Lasbleiz et al.,
271 2014).

272 Nutrient drawdown lower than the Redfield ratio has been observed previously in the
273 Southern Ocean. During the artificial iron fertilization experiment EIFEX, an apparent
274 differential consumption of $\Delta(\text{NO}_3^-):\Delta(\text{PO}_4^{3-})$ of 6.4 was reported (Smetacek et al., 2012).
275 Arrigo et al.(Arrigo, 1999) and (De Baar et al., 1997) determined a nutrient drawdown ratio in
276 diatom blooms of 9.7 and 4.4-6.1, respectively. Near Crozet, the removal of NO_3^- versus
277 PO_4^{3-} measured in situ and during iron addition experiments revealed that the ratio was
278 inversely related to the proportion of diatoms in the phytoplankton community (Moore et al.,
279 2007). All these studies confirm the impact of diatom blooms on nutrient stoichiometry in the
280 surface layer. However, the interpretations of these observations are diverse. (De Baar et al.,
281 1997) suggested that the preferential drawdown of PO_4^{3-} during the bloom of *Fragiliaropsis*
282 *keruelensis* in the PF could be due to the reduction of nitrate reductase activity by iron
283 limitation or due to the dominance of *Fragiliaropsis kerguelensis* with low N:P ratios
284 considered as a specific physiological trait. These hypotheses could not explain our
285 observations because the stations with a nutrient drawdown anomaly were located in an iron
286 fertilized region and the diatom community was not dominated by *Fragiliaropsis kerguelensis*
287 but rather by *Chaetoceros (Hylochaete)* spp, *Pseudo-nitzschia* spp and *Centric* sp (Lasbleiz et
288 al., 2014).

289 Thus, we interpret the positive values of N^* as a result of the preferential uptake of
290 PO_4^{3-} versus NO_3^- by fast growing diatoms. Diatoms have a mean elemental N:P
291 stoichiometry of 10 ± 4 (Sarhou et al., 2005) that differs from the Redfield value. Indeed, the

292 elemental particulate matter composition determined at the stations with positive N^* during
293 KEOPS2 (Lasbleiz et al., 2014) exhibits a mean ratio of PON:POP of 10.5 ± 3.3 which is
294 consistent with the observed nutrient drawdown $\Delta(\text{NO}_3^-) : \Delta(\text{PO}_4^{3-})$ of 8. We suggest that the
295 preferential allocation of resources to the P-rich assembly of the cell machinery by
296 exponentially growing cells is the most likely explanation for our observations (Klausmeier et
297 al., 2004). The anomaly observed for the present data set is not linked to a particular species
298 but to general traits of the diatom community responding to iron fertilization.

299 As a variant of N^* , the tracer DIN_{xs} , takes into account NO_2^- and NH_4^+ (Hansell et al.,
300 2007), but none of those tracers consider the organic pools of N and P. Landolfi et al. (2008)
301 have defined the tracer $\text{TN}_{\text{xs}} = [\text{TDN}] - 16[\text{TDP}]$ and have shown that the dissolved organic
302 fraction significantly contributes to changes in TN_{xs} . For example, relying on N^* only, can
303 lead to an underestimation of N_2 fixation at the global scale (Landolfi et al., 2008). In the case
304 of KEOPS2, the contribution of DON and DOP to TDN and TDP reached 30%. We have
305 therefore considered TDN and TDP at all KEOPS2 stations where these measurements were
306 available (Fig. 9b). Plotting TDN as a function of TDP ($\text{TDN} = f(\text{TDP})$) reveals more
307 dispersion of the data than $\text{NO}_3^- = f(\text{PO}_4^{3-})$, mainly due to the lower analytical precision for
308 DOP and DON determinations. Still, clear trends are detectable. TN_{xs} values were negative
309 for most stations and depths, and relatively constant in the layer 0-500m. As for N^* the
310 stations north of the PF had higher TN_{xs} in the layer 0-100m.

311 When a water parcel is considered, N^* is affected by the redistribution of N and P
312 between the inorganic and the organic pools, whereas TN_{xs} is only affected by net non-
313 Redfield sources or sinks of N and P. Consequently, the positive anomaly observed for TN_{xs}
314 in surface waters north of the PF can be explained by three possible mechanisms: Deposition
315 of N rich material from the atmosphere, N_2 fixation and export of P rich material. The region
316 of Kerguelen receives low quantities of atmospheric material (Heimburger et al., 2012;

317 Wagener et al., 2008) which is mainly from natural origin, such as desert dust, that contains
318 little nitrogen compared to phosphorus (Zamora et al., 2013). This is confirmed by the low N
319 deposition rate estimated around Crozet Island ($2 \text{ nmol m}^{-2} \text{ d}^{-1}$; Planquette et al., 2007). We
320 can therefore refute the deposition of N rich material as the cause of the TN_{xs} anomaly. The
321 second hypothesis involves N_2 fixation. To date, N_2 fixation was not reported to occur in the
322 cold waters of the Southern Ocean. However, during KEOPS2 detectable N_2 fixation rates
323 were measured at different stations with a few exceptionally high values ($\sim 250 \text{ } \mu\text{mol m}^{-2} \text{ d}^{-1}$)
324 in the mixed layer of station F-L (González et al. this issue)). Such high fixation rates could
325 contribute to an enrichment of about 1% of TDN that is not enough to create the observed
326 anomaly. If N_2 fixation was a dominant process driving the N:P stoichiometry at this station,
327 POM elemental composition should be also affected. Generally, N_2 fixing microorganisms
328 have a high N:P ratio (Laroche, J. and Breitbarth, E., 2005). Such high ratios are at odds with
329 the low N:P measured in the POM at station F-L (Lasbleiz et al., 2014). The third hypothesis
330 for explaining the anomaly relies on the export of P rich material from the mixed layer. We do
331 not have direct measurements of N:P in the exported material, but we already mentioned
332 above that the elemental composition of particulate matter at station F-L yielded the lowest
333 N:P ratio in POM (Lasbleiz et al., 2014). This provides support that the export of P rich
334 material could result in high TN_{xs} values north of the PF. We propose that the anomaly of
335 TN_{xs} results from the imprint on stoichiometry of the diatom bloom which consumed and
336 exported phosphorus with a N/P ratio below the Redfield value.

337 During KEOPS2 rapidly growing diatom blooms were also sampled at other stations
338 located south of the PF, but anomalies similar to those at F-L were not observed. We discuss
339 here the case of stations A3 and E-4W, which had similar chlorophyll concentrations as F-L.
340 Station A3 had a contribution of diatoms to carbon biomass and dominant diatom species
341 similar to F-L (these observations are not available for E4-W) (Lasbleiz et al., 2014). There is

342 no reason that the physiological features of exponentially growing diatoms as revealed for
343 station F-L do not apply to the diatoms growing at stations A3 and E4-W. It is, however,
344 possible that the resulting effect is not large enough to translate into N^* or TN_{xs} anomalies. A
345 possible explanation could be the differences in the age of the blooms. The stoichiometry
346 would be less affected in a younger bloom as compared to a bloom of longer duration. This
347 hypothesis cannot be fully verified due to the poor temporal resolution of the satellite ocean
348 color images available (see supplementary animations provided in Trull et al., 2014. Another
349 or complementary explanation is the difference in the mixed layer depths that were 50 m and
350 150 m at stations F-L and A3-2, respectively. Such a deep mixed layer as observed at station
351 A3-2 resulted likely from a deep episodic mixing event generated by strong wind prevailing
352 during the day preceding our visit. The deepening could have dampened the anomaly by
353 diluting and mixing the affected water parcel with underlying water having a typical
354 stoichiometry (e.g. N^* or TN_{xs} around -3).

355 In February 2013, two years after the KEOPS2 cruise, we had the possibility to return to two
356 sites visited during KEOPS2 (stations A3 and TNS-6), and obtain measurements for the
357 concentrations of NO_3^- and PO_4^{3-} . These data, in combination with KEOPS2 data allowed us
358 to compare N^* during two different seasons (Fig. 10). In the mixed layer, little changes of N^*
359 were observed between spring and summer. However, in summer, N^* exhibited a clear
360 subsurface minimum between 100-200 m, at both stations. Denitrification is a process that
361 could produce this subsurface feature. But denitrification would require low oxygen
362 concentrations that are not observed at these stations. In a general manner, preferential
363 remineralisation of P versus N in the water column is supported by an increase of N:P in high
364 molecular dissolved organic matter (Clark, L. L. et al., 1998) in particulate matter (Copin-
365 Montegut and Copin-Montegut, 1978) and in supernatant of sediment trap material (Lourey et
366 al., 2003). The observation of the N^* subsurface minimum at the end of the season, but not at

367 the beginning implies a temporal cumulative effect. The minimum is located just below the
368 mixed layer in the region of the pycnocline that presents the highest density gradient. This
369 could represent a zone with a higher residence time for sinking particles resulting in an
370 accumulation of biomass. Additional evidence for intensive remineralization at shallow
371 depths at this location is provided by strong attenuation of the particles fluxes as observed
372 with moored sediment trap (Rembauville et al . this issue).Consequently, the remineralization
373 would also be increased in this layer compared to the rest of the water column resulting in a
374 higher accumulation of PO_4^{3-} relative to NO_3^- . This effect might be amplified by the
375 occurrence of particulate organic matter with low N:P ratio resulting from diatom
376 accumulation at the pycnocline. The subsurface minimum being located above 200 m depth, it
377 is erased when the winter mixing occurs.

378 To our knowledge such a subsurface minimum has not be reported in the Southern Ocean.
379 This could be due to the limited studies that investigate concurrently dissolved N and P
380 biogeochemistry, and due to the lack of samples collected at the appropriate vertical and
381 temporal time scale. Our finding raises several further questions. Is the subsurface minimum
382 of N^* a particular feature of iron fertilized regions? What is the link between its occurrence
383 and the strength of stratification of the water column? And what is the role of this layer in the
384 remineralisation of carbon? These questions argue for future detailed investigations of the
385 cycling of both elements in the upper layer of the Southern Ocean.

386

387

388 **Figure captions**

389

390 **Figure 1:** Map of the KEOPS2 study area. The locations of the stations are marked by colored

391 dots. Blue indicates the stations of the North-South transect (TNS), green indicates the

392 stations of the East-West transect (TEW), orange indicates the stations E located in the

393 meander of the Polar Front (zoom panel). Red stands for other stations located in the fertilized

394 region and black stands for the station located in the HNLC region. Detailed positions of the

395 stations are given in supplementary Table 1.

396

397 **Figure 2:** Vertical sections of dissolved nitrogen and phosphorus species along the East-West

398 transect (TEW). (a) Nitrate, (b) Ammonium, (c) Phosphate, (d), Nitrite, (e) Dissolved organic

399 nitrogen, (f) Dissolved organic phosphorus. The isolines for sigma-theta are plotted on each

400 panel.

401

402 **Figure 3:** Vertical sections of dissolved nitrogen and phosphorus species along the North-

403 South transect (TNS). (a) Nitrate, (b) Ammonium), (c) Phosphate, (d), Nitrite, (e) Dissolved

404 organic nitrogen, (f) Dissolved organic phosphorus. The isolines for sigma-theta are plotted

405 on each panel.

406

407

408 **Figure 4:** Dissolved nitrogen speciation at station A3-1 (a, b) and at station A3-2 (c, d) during

409 KEOPS2. Depth profiles of temperature and sigma-theta are plotted on each panel.

410

411 **Figure 5:** Dissolved nitrogen speciation at stations F-L and F-S during KEOPS2.

412

413 **Figure 6:** Dissolved nitrogen speciation at station R-2.

414

415 **Figure 7 :** Temporal variability of the vertical profiles of concentrations of NO_3^- (a) and
416 PO_4^{3-} (b) for stations located in the meander of the Polar Front. Details for profiles of
417 KEOPSMOOR (February 2013) and ANTARES3 (October 1995) are provided in the text.

418

419 **Figure 8:** Temporal variability of the vertical profiles of concentrations of NO_3^- (a) and PO_4^{3-}
420 (b) at the station A3.

421

422 **Figure 9:** (a) Comparison of concentrations of NO_3^- versus PO_4^{3-} . Dots denote the samples
423 and lines show different values of $\text{N}^* = \text{NO}_3^- - r_{\text{N:P}} \text{PO}_4^{3-}$ (b) Comparison of concentrations of
424 TDN versus TDP, dots denote the samples and lines show different values of $\text{TN}_{\text{xs}} = \text{TDN} -$
425 $r_{\text{N:P}} \text{TDP}$.

426

427 **Figure 10:** Depth profiles of N^* at stations A3 (a) and TNS-6 (b) for the month of November
428 (in red) and February (in blue). Vertical profiles of sigma-theta are shown with the same color
429 code.

430

431 **Acknowledgment :**

432 We thank the chief scientist Bernard Quéguiner, the captain Bernard Lassiette and crew of the
433 R/V Marion Dufresne for their support aboard. We thank C. Lo Monaco for providing us
434 with the CTD profiles of KEOPSMOOR. This work was supported by the French Research
435 program of INSU-CNRS LEFE-CYBER (Les enveloppes fluides et l'environnement –Cycles
436 biogéochimiques, environnement et ressources), the French ANR (Agence Nationale de la

437 Recherche, SIMI-6 program, ANR-10-BLAN-0614), the French CNES (Centre National
438 d'Etudes Spatiales) and the French Polar Institute IPEV (Institut Polaire Paul–Emile Victor).

439

440 **Bibliography**

441 Aminot, A. and K erouel, R.: Dosage automatique des nutriments dans les eaux marines :
442 m ethodes en flux continu, Ifremer., 2007.

443 Arrigo, K. R.: Phytoplankton Community Structure and the Drawdown of Nutrients and CO₂
444 in the Southern Ocean, *Science*, 283(5400), 365–367, doi:10.1126/science.283.5400.365,
445 1999.

446 De Baar, H. J. W., Van Leeuwe, M. A., Scharek, R., Goeyens, L., Bakker, K. M. J. and
447 Fritsche, P.: Nutrient anomalies in *Fragilariopsis kerguelensis* blooms, iron deficiency and the
448 nitrate/phosphate ratio (A. C. Redfield) of the Antarctic Ocean, *Deep Sea Res. Part II Top.*
449 *Stud. Oceanogr.*, 44(1-2), 229, 1997.

450 Blain, S., Qu eguiner, B., Armand, L., Belviso, S., Bombled, B., Bopp, L., Bowie, A., Brunet,
451 C., Brussaard, K., Carlotti, F., Christaki, U., Corbi ere, A., Durand, I., Ebersbach, F., Fuda, J.
452 L., Garcia, N., Gerringa, L. J. A., Griffiths, F. B., Guigue, C., Guillerm, C., Jacquet, S.,
453 Jeandel, C., Laan, P., Lef evre, D., Lomonaco, C., Malits, A., Mosseri, J., Obernosterer, I.,
454 Park, Y. H., Picheral, M., Pondaven, P., Remenyi, T., Sandroni, V., Sarthou, G., Savoye, N.,
455 Scouarnec, L., Souhault, M., Thuillers, D., Timmermans, K. R., Trull, T., Uitz, J., Van-Beek,
456 P., Veldhuis, M. J. W., Vincent, D., Viollier, E., Vong, L. and Wagener, T.: Effect of natural
457 iron fertilisation on carbon sequestration in the Southern Ocean, *Nature*, 446(7139), 1070–
458 1075, doi:doi:10.1038/nature05700, 2007.

459 Boyd, P. W., Jickells, T., Law, C., Blain, S., Boyle, E. A., Buesseler, K. O., Coale, K. H.,
460 Cullen, J. J., De Baar, H. J. W., Follows, M., Harvey, M., Lancelot, C., Levasseur, M.,
461 Owens, N. J. P., Pollard, D. A., Rivkin, R. B., Sarmiento, J. L., Schoemann, V., Smetacek, V.,
462 Takeda, S., Tsuda, A., Turner, D. R. and Watson, A.: Mesoscale iron enrichment experiments
463 1993-2005: Synthesis and future directions, *Science*, 315, 612–617,
464 doi:10.1126/science.1131669, 2007.

465 Clark, L. L., Ingall, E. and Benner, R.: Marine phosphorus isselectively remineralized, *Nature*,
466 393, 426, 1998.

467 Copin-Montegut, C. and Copin-Montegut, G.: the chemistry of particulate matter from the
468 south indien and antarctic ocean, *Deep Sea Res.*, 25, 911–931, 1978.

469 Deutsch, C. and Weber, T.: Nutrient Ratios as a Tracer and Driver of Ocean Biogeochemistry,
470 *Annu. Rev. Mar. Sci.*, 4(1), 113–141, doi:10.1146/annurev-marine-120709-142821, 2012.

471 Gnanadesikan, A., Sarmiento, J. L. and Slater, R. D.: Effects of patchy ocean fertilization on
472 atmospheric carbon dioxide and biological production, *Glob. Biogeochem. Cycles*, 17(2),
473 1050, doi:10.1029/2002GB001940, 2003.

474 Hansell, D. A., Olson, D. B., Dentener, F. and Zamora, L. M.: Assessment of excess nitrate
475 development in the subtropical North Atlantic, *Maine Chem.*, 206, 562–579, 2007.

476 Hart, T. J.: Phytoplankton periodicity in Antarctic surface water, *Discov. Rep.*, VIII, 1–268,
477 1942.

478 Heimburger, A., Losno, R., Triquet, S., Dulac, F. and Mahowald, N.: Direct measurements of
479 atmospheric iron, cobalt, and aluminum-derived dust deposition at Kerguelen Islands, *Glob.*
480 *Biogeochem. Cycles*, 26(4), GB4016, doi:10.1029/2012GB004301, 2012.

481 Holmes, R. M., Aminot, A., K erouel, R., Hooker, B. and peterson, B.: a simple and precise
482 method for measuring ammonium in marine and freshwater ecosystem, , 56(10), 1801–1808,
483 1999.

484 Jenkins, B. D., Gordon, L. I. and Nelson, D. M.: Nutrient depletion indicates high primary
485 productivity in the Weddel Sea, *Nature*, 309, 51–54, 1984.

486 Klausmeier, C. A., Litchman, E., Daufresne, T. and Levin, S. A.: Optimal nitrogen-to-
487 phosphorus stoichiometry of phytoplankton, *Nature*, 429(6988), 171–174,
488 doi:10.1038/nature02454, 2004.

489 Landolfi, A., Oschlies, A. and Sanders, R.: Organic nutrients and excess nitrogen in the North
490 Atlantic subtropical gyre, *Biogeosciences*, 5(5), 1199–1213, doi:10.5194/bg-5-1199-2008,
491 2008.

492 Laroche, J. and Breitbarth, E.: Importance of the diazotrophs as a source of new nitrogen in
493 the ocean, *J. Sea Res.*, 53(1-2), 67–91, 2005.

494 Lasbleiz, M., Leblanc, K., Blain, S., Ras, J., Cornet-Barthaux, V., H elias Nunige, S. and
495 Qu eguiner, B.: Pigments, elemental composition (C, N, P, and Si), and stoichiometry of
496 particulate matter in the naturally iron fertilized region of Kerguelen in the Southern Ocean,
497 *Biogeosciences*, 11(20), 5931–5955, doi:10.5194/bg-11-5931-2014, 2014.

498 Lourey, M. J., Trull, T. W. and Sigma-thetan, D. M.: Sensitivity of $\delta^{15}\text{N}$ of nitrate, surface
499 suspended and deep sinking particulate nitrogen to seasonal nitrate depletion in the Southern
500 Ocean, *Glob. Biogeochem. Cycles*, 17(3), n/a–n/a, doi:10.1029/2002GB001973, 2003.

501 Lourey, M. and Trull, T. W.: seasonal nutrient depletion and carbon export in the subantarctic
502 and polar frontal zones of the Southern Ocean, *J. Geophys. Res. Oceans*, 106(C12), 31463–
503 31487, 2001.

504 Marshall, J. and Speer, K.: Closure of the meridional overturning circulation through
505 Southern Ocean upwelling, *Nat. Geosci.*, 5(3), 171–180, doi:10.1038/ngeo1391, 2012.

506 Martinez-Garcia, A., Sigma-thetan, D. M., Ren, H., Anderson, R. F., Straub, M., Hodell, D.
507 A., Jaccard, S. L., Eglinton, T. I. and Haug, G. H.: Iron Fertilization of the Subantarctic Ocean
508 During the Last Ice Age, *Science*, 343(6177), 1347–1350, doi:10.1126/science.1246848,
509 2014.

510 Martin, J. M. and Fitzwater, S. E.: Iron deficiency limits phytoplankton growth in the north-
511 east Pacific subarctic, *Nature*, 331, 341–343, 1988.

512 Michaels, A. F., Olson, D., Sarmiento, J., Ammerman, J. W., Fanning, K. A., Jahnke, R. A.,
513 Knap, A. H., Lipschultz, F. and Prospero, J. M.: Inputs, losses and transformations of nitrogen
514 and phosphorus in the pelagic North Atlantic Ocean, *Biogeochemistry*, 35, 181–226, 1996.

515 Minas, H. J. and Minas, M.: : Net community production in “High Nutrient-Low
516 Chlorophyll” waters of the tropical and antarctic oceans: grazing versus iron hypothesis,
517 *Oceanol. Acta*, 15(2), 145–162, 1992.

518 Moore, C. M., Hickman, A. E., Poulton, A. J., Seeyave, S. and Lucas, M. I.: Iron–light
519 interactions during the CROZet natural iron bloom and EXport experiment (CROZEX): II—
520 Taxonomic responses and elemental stoichiometry, *Deep Sea Res. Part II Top. Stud.*
521 *Oceanogr.*, 54(18-20), 2066–2084, doi:10.1016/j.dsr2.2007.06.015, 2007.

522 Park, Y.-H., Durand, I., Kestenare, E., Rougier, G., Zhou, M., d’ Ovidio, F., Cotté, C. and
523 Lee, J.-H.: Polar Front around the Kerguelen Islands: An up-to-date determination and
524 associated circulation of surface/subsurface waters, *J. Geophys. Res. Oceans*,
525 doi:10.1002/2014JC010061, 2014.

526 Planquette, H., Statham, P. J., Fones, G., Charette, M. A., Moore, C. M., Salter, I., Nédélec, F.
527 H., Taylor, S. L., French, M., Baker, A. R., Mahowald, N. and Jickells, T. D.: Dissolved iron
528 in the vicinity of the Crozet islands, Southern Ocean, *Deep-Sea Res. II*, 54, 1999–2019, 2007.

529 Redfield, A. C., Ketchum, B. H. and Richards, F. A.: The influence of organism on the
530 composition of seawater, in *The Sea*, Hill N. M., New York., 1963.

531 Sarmiento, J. L., Gruber, N., Brzezinsky, M. A. and Dunne, J. P.: High-latitude controls of
532 thermocline nutrients and low latitude biological productivity, *Nature*, 427, 2004.

533 Sarmiento, J. L. and Orr, J. C.: Three-dimensional simulations of the impact of Southern
534 Ocean nutrient depletion on atmospheric CO₂ and ocean chemistry, *Limnol. Oceanogr.*, 36,
535 1928–1950, 1991.

536 Sarthou, G., Timmermans, K. R., Blain, S. and Treguer, P.: Growth physiology and fate of
537 diatoms in the ocean: a review, *J. Sea Res.*, 53(1-2), 25, 2005.

538 Sigma-thetan, D. M. and Boyle, E. A.: Glacial/interglacial variations in atmospheric carbon
539 dioxide, *Science*, 407, 859–869, 2000.

540 Smetacek, V., Klaas, C., Strass, V. H., Assmy, P., Montresor, M., Cisewski, B., Savoye, N.,
541 Webb, A., d’ Ovidio, F., Arrieta, J. M., Bathmann, U., Bellerby, R., Berg, G. M., Croot, P.,

542 Gonzalez, S., Henjes, J., Herndl, G. J., Hoffmann, L. J., Leach, H., Losch, M., Mills, M. M.,
543 Neill, C., Peeken, I., Röttgers, R., Sachs, O., Sauter, E., Schmidt, M. M., Schwarz, J.,
544 Terbrüggen, A. and Wolf-Gladrow, D.: Deep carbon export from a Southern Ocean iron-
545 fertilized diatom bloom, *Nature*, 487(7407), 313–319, doi:10.1038/nature11229, 2012.

546 Trull, T. W., Davies, D. M., Dehairs, F., Cavagna, A.-J., Lasbleiz, M., Laurenceau, E. C., d'
547 Ovidio, F., Planchon, F., Leblanc, K., Quéguiner, B. and Blain, S.: Chemometric perspectives
548 on plankton community responses to natural iron fertilization over and downstream of the
549 Kerguelen Plateau in the Southern Ocean, *Biogeosciences Discuss.*, 11(9), 13841–13903,
550 doi:10.5194/bgd-11-13841-2014, 2014.

551 Wagener, T., Guieu, C., Losno, R., Bonnet, S. and Mahowald, N.: Revisiting atmospheric
552 dust export to the southern hemisphere ocean: biogeochemical implication, *Glob.*
553 *Biogeochem. Cycles*, 22(GB2006), doi:10.1029/2007GB002984., 2008.

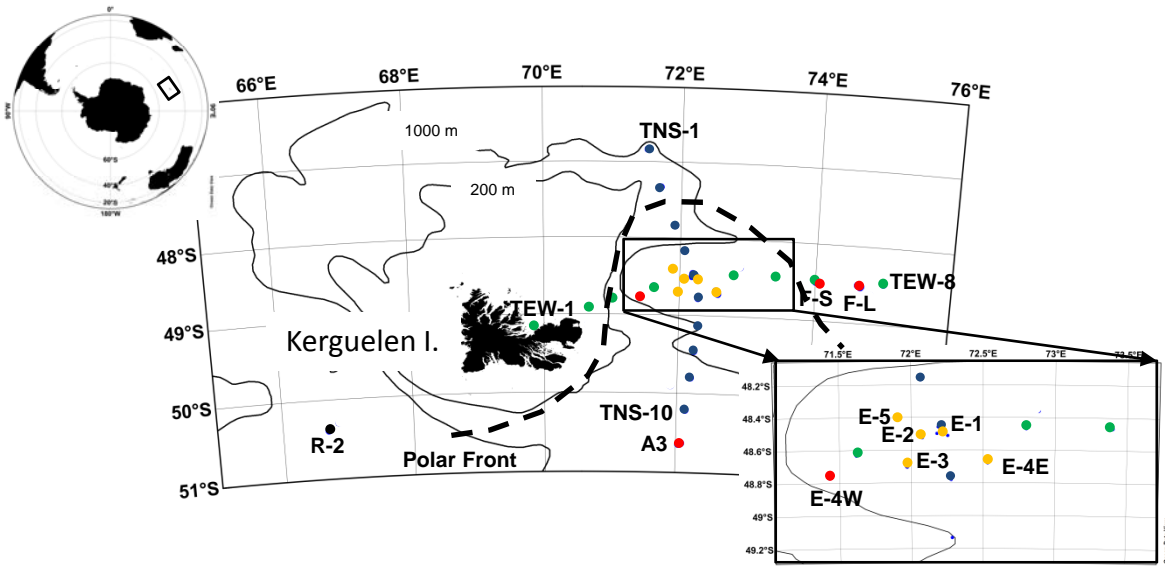
554 Wang, X., Matear, R. J. and Trull, T. W.: Nutrient utilization ratios in the Polar Frontal Zone
555 in the Australian sector of the Southern Ocean: A model., *Glob. Biogeochem. Cycles*, 17(1),
556 n/a–n/a, doi:10.1029/2002GB001938, 2003.

557 Weber, T. S. and Deutsch, C.: Ocean nutrient ratios governed by plankton biogeography,
558 *Nature*, 467(7315), 550–554, doi:10.1038/nature09403, 2010.

559 Zamora, L. M., Prospero, J. M., Hansell, D. A. and Trapp, J. M.: Atmospheric P deposition to
560 the subtropical North Atlantic: sources, properties, and relationship to N deposition, *J.*
561 *Geophys. Res. Atmospheres*, 118(3), 1546–1562, doi:10.1002/jgrd.50187, 2013.

562 Zhou, M., Zhu, Y., d' Ovidio, F., Park, Y.-H., Durand, I., Kestenare, E., Sanial, V., Van-
563 Beek, P., Queguiner, B., Carlotti, F. and Blain, S.: Surface currents and upwelling in
564 Kerguelen Plateau regions, *Biogeosciences Discuss.*, 11(5), 6845–6876, doi:10.5194/bgd-11-
565 6845-2014, 2014.

566



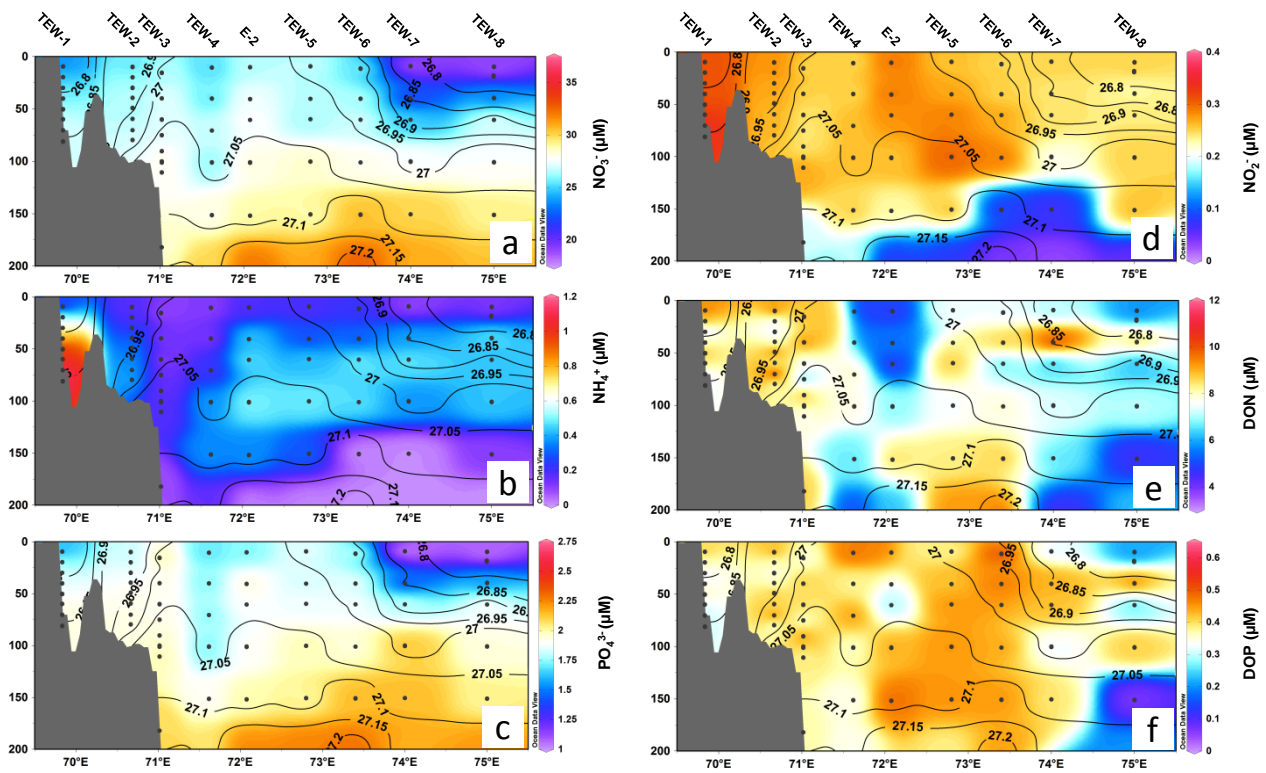


Figure 2

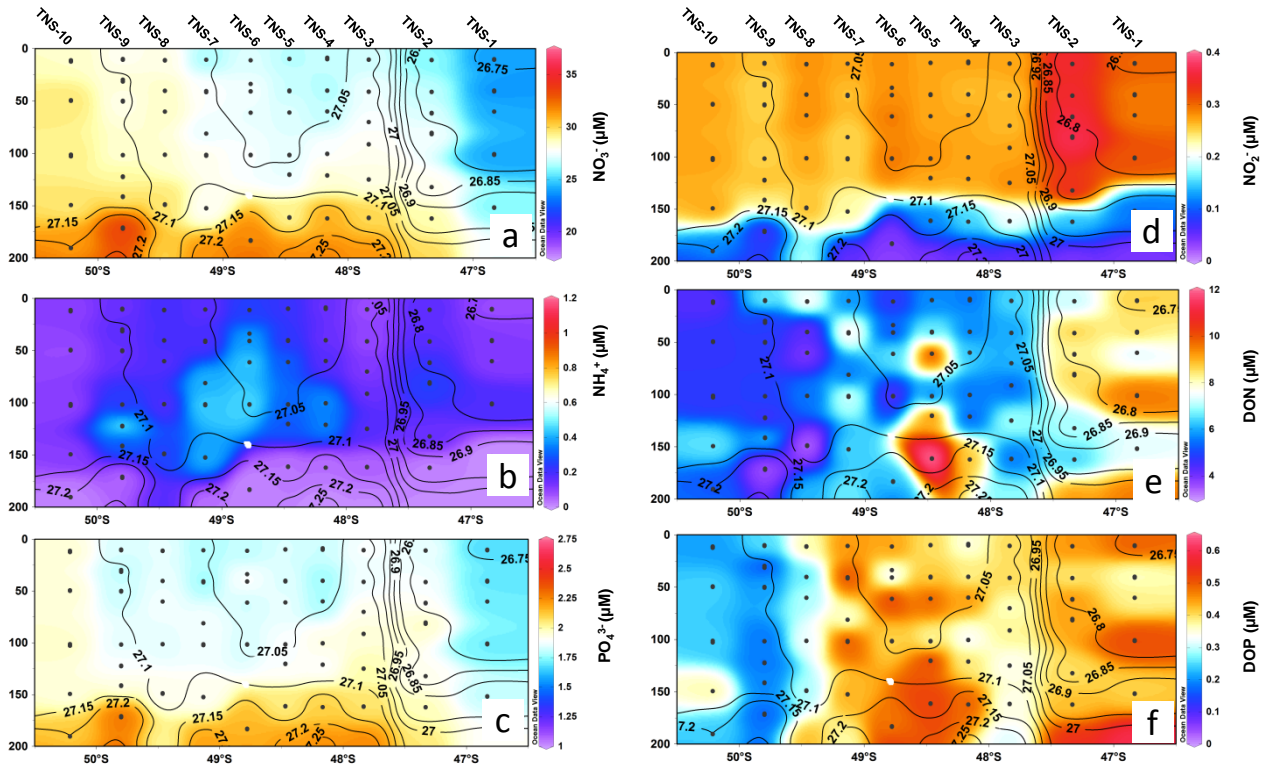
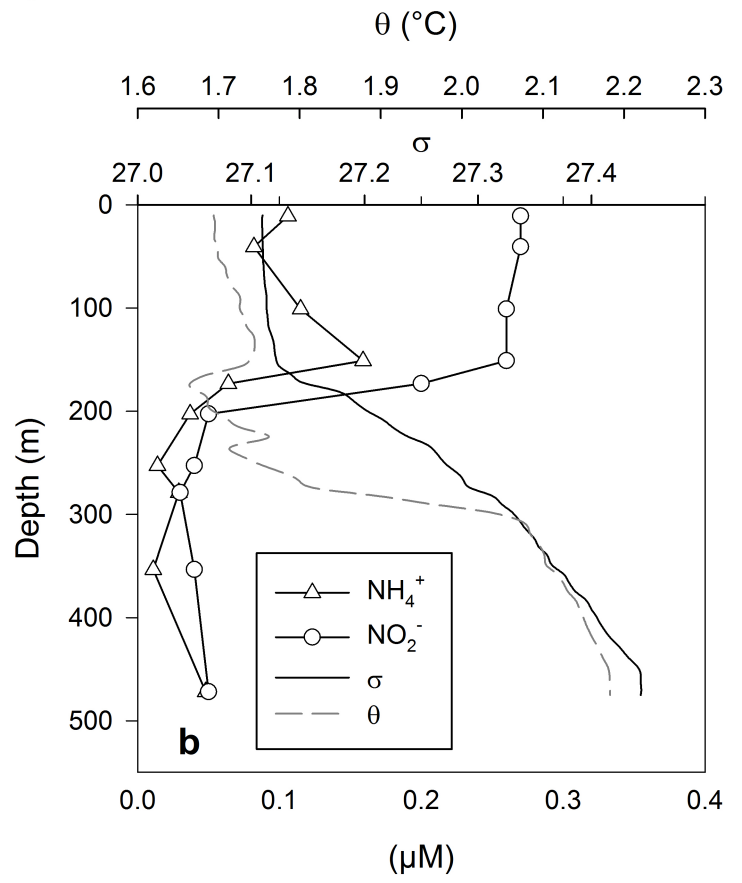
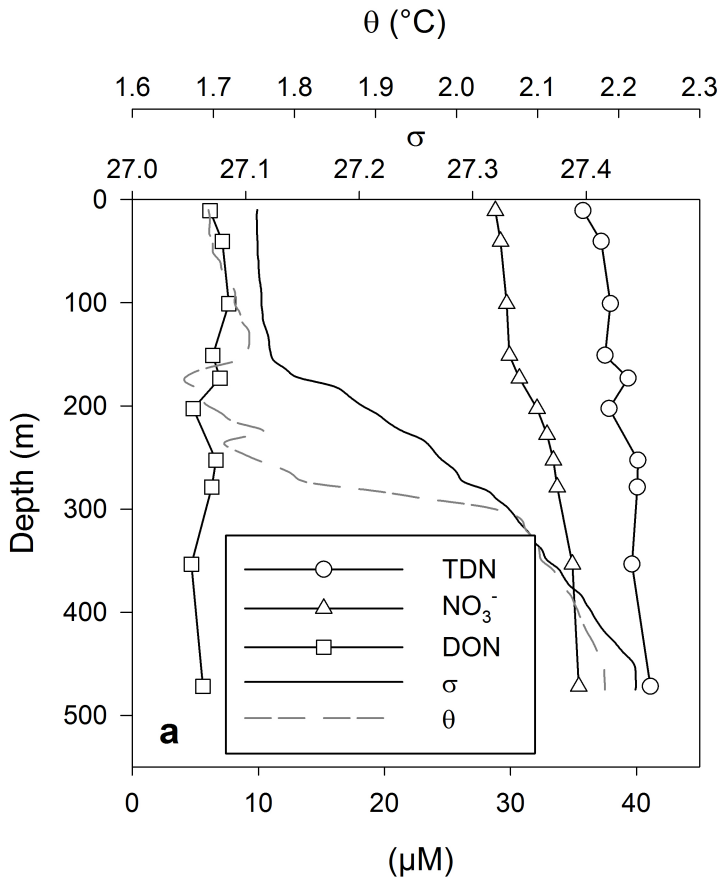


Figure 3

A3-1



A3-2

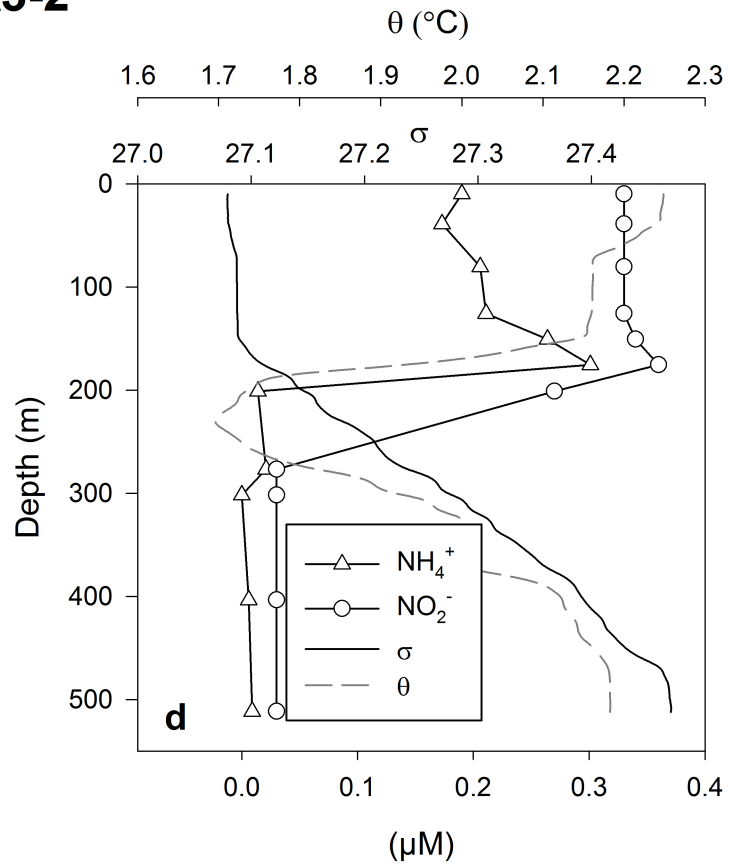
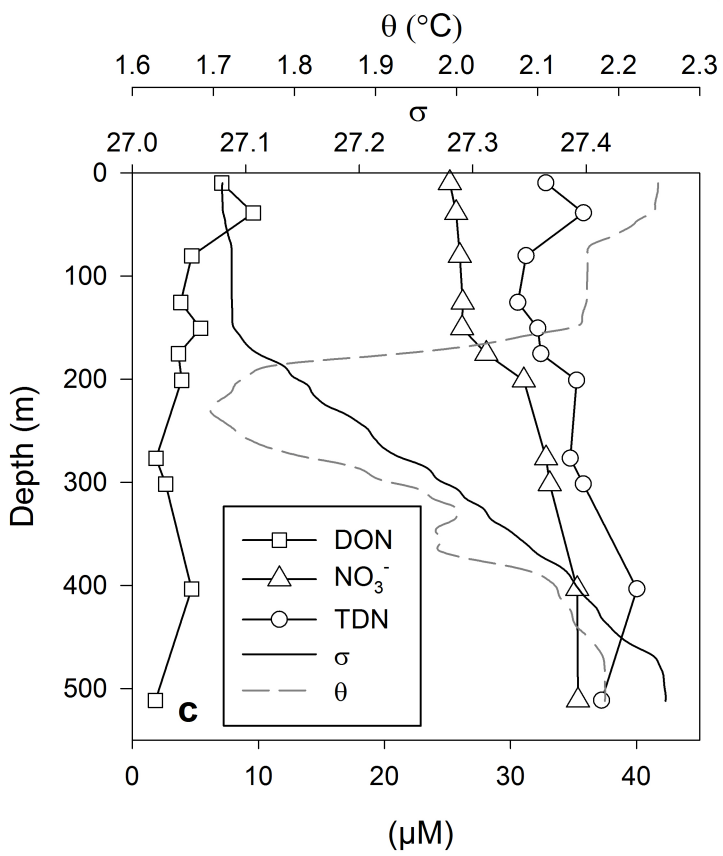


Figure 4

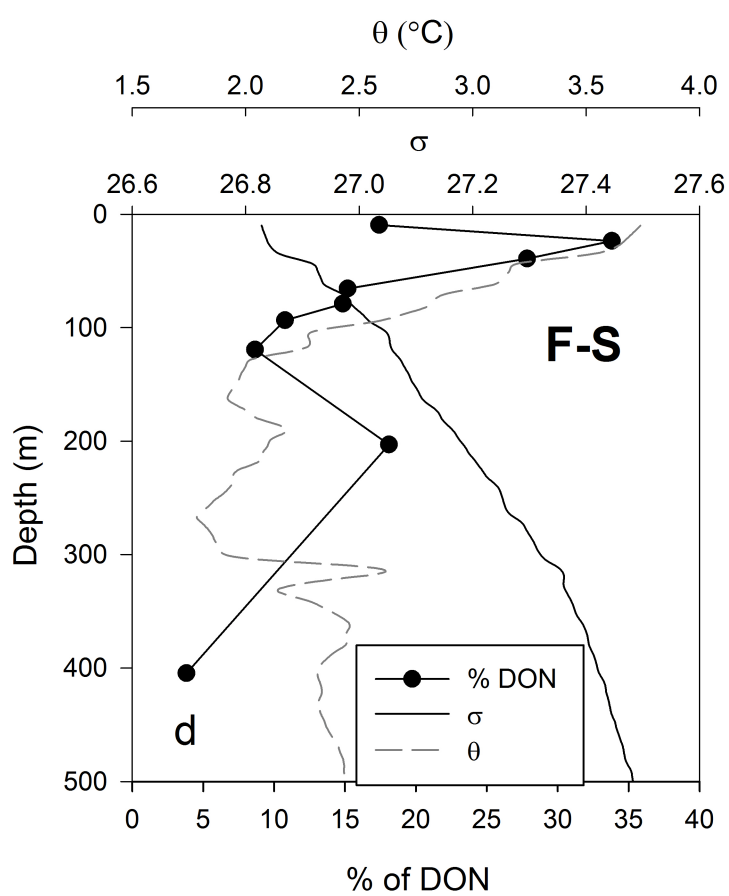
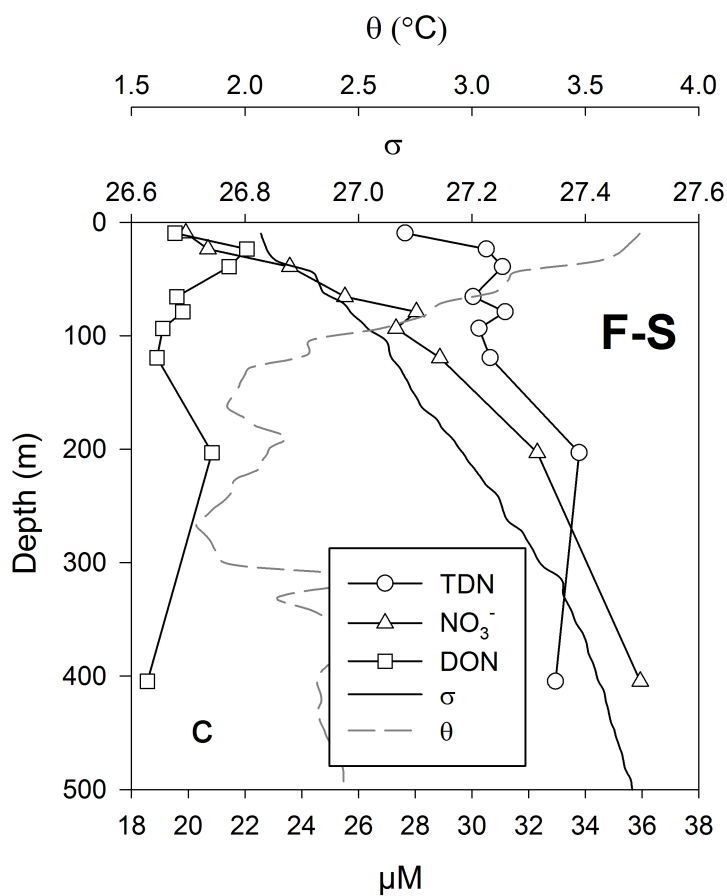
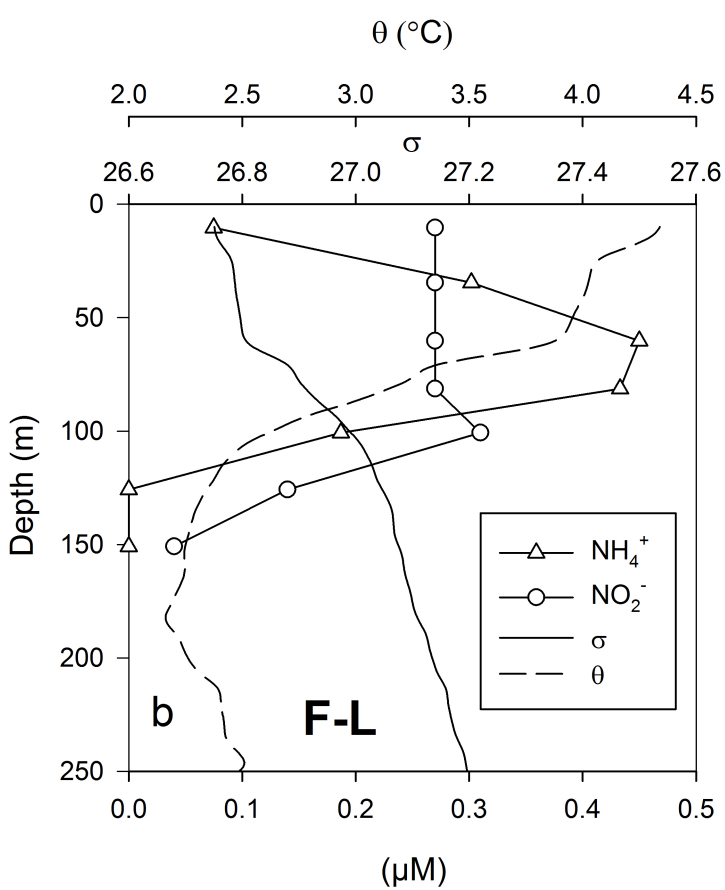
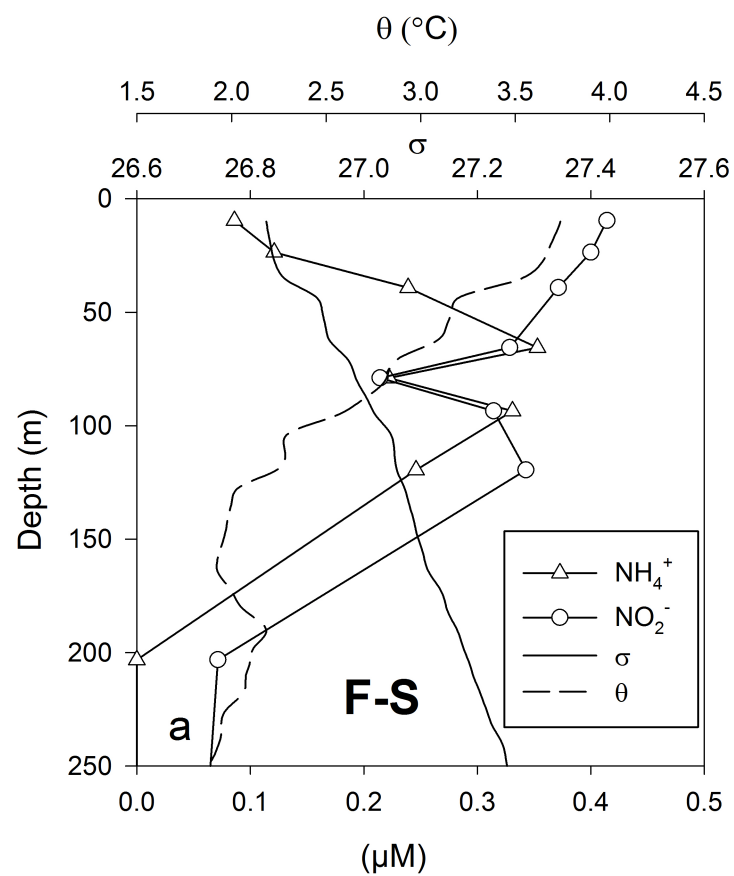


Figure 5

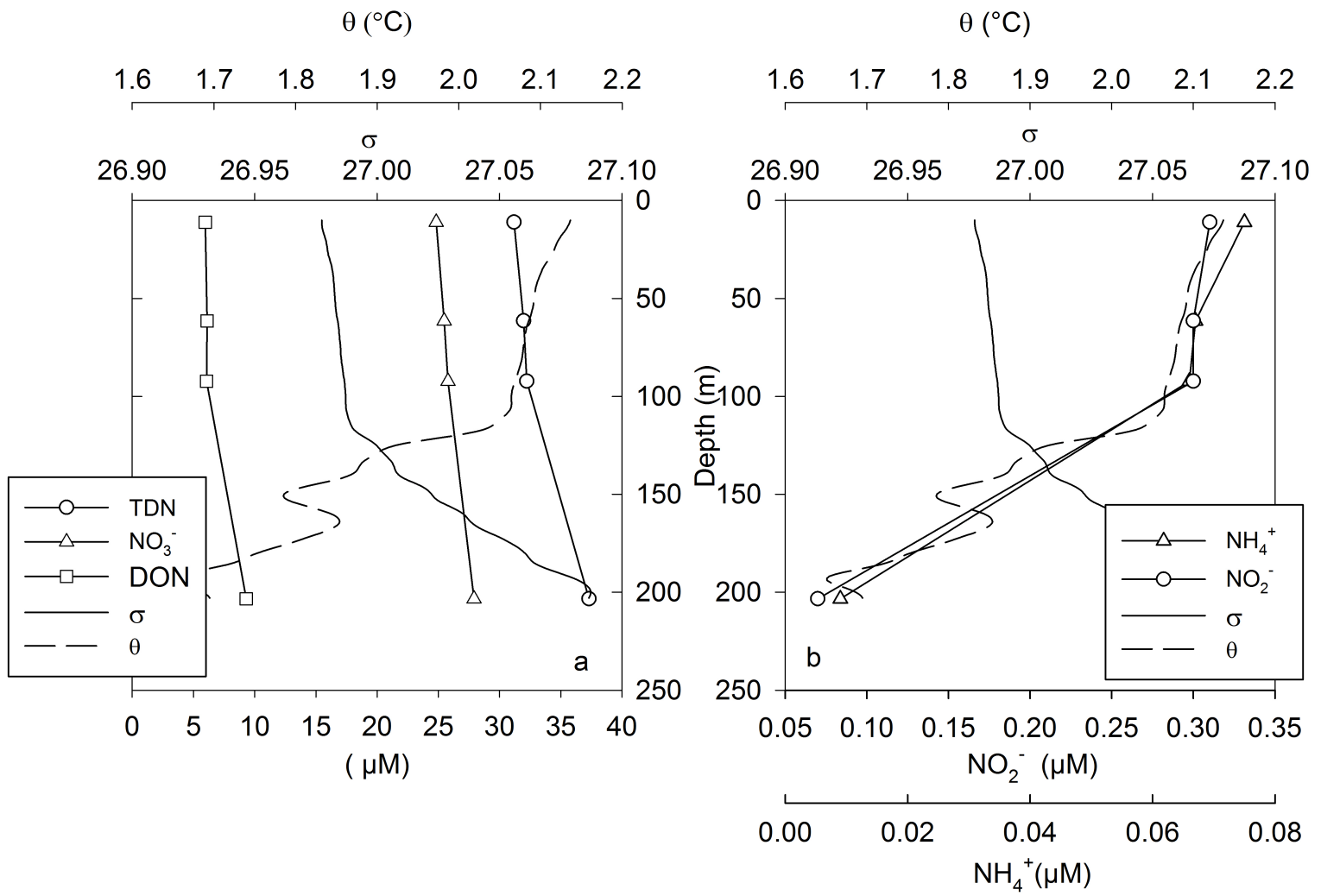


Figure 6

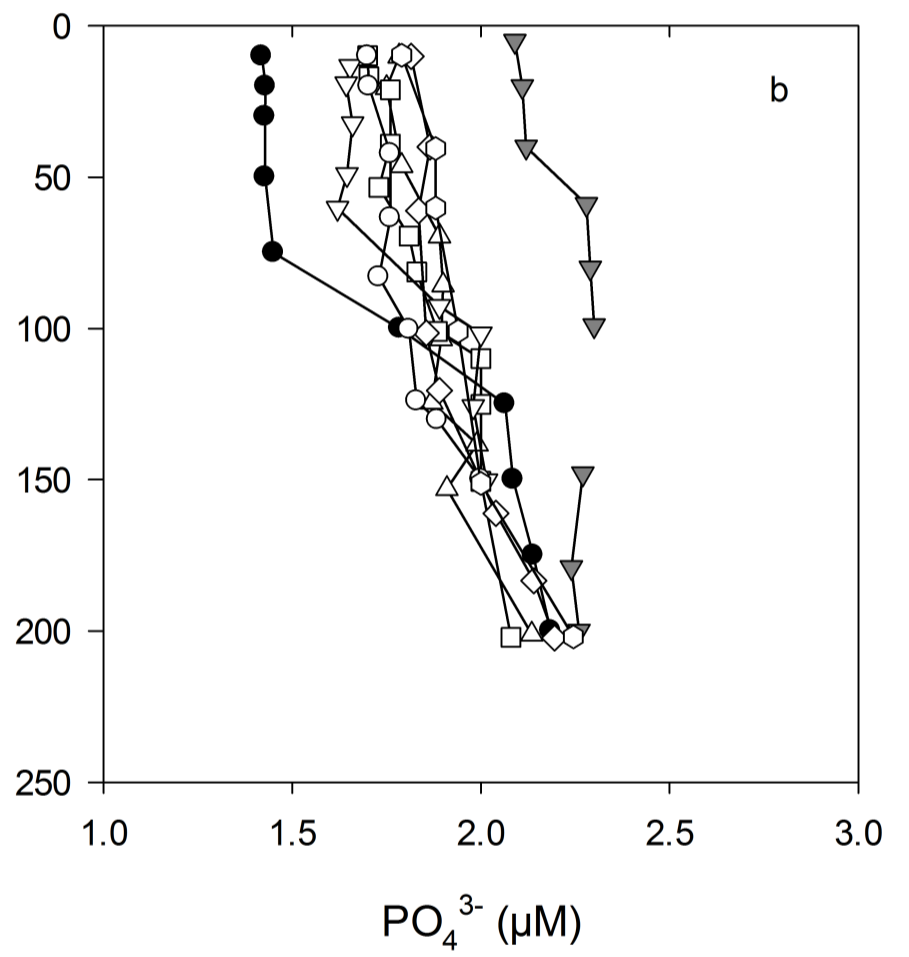
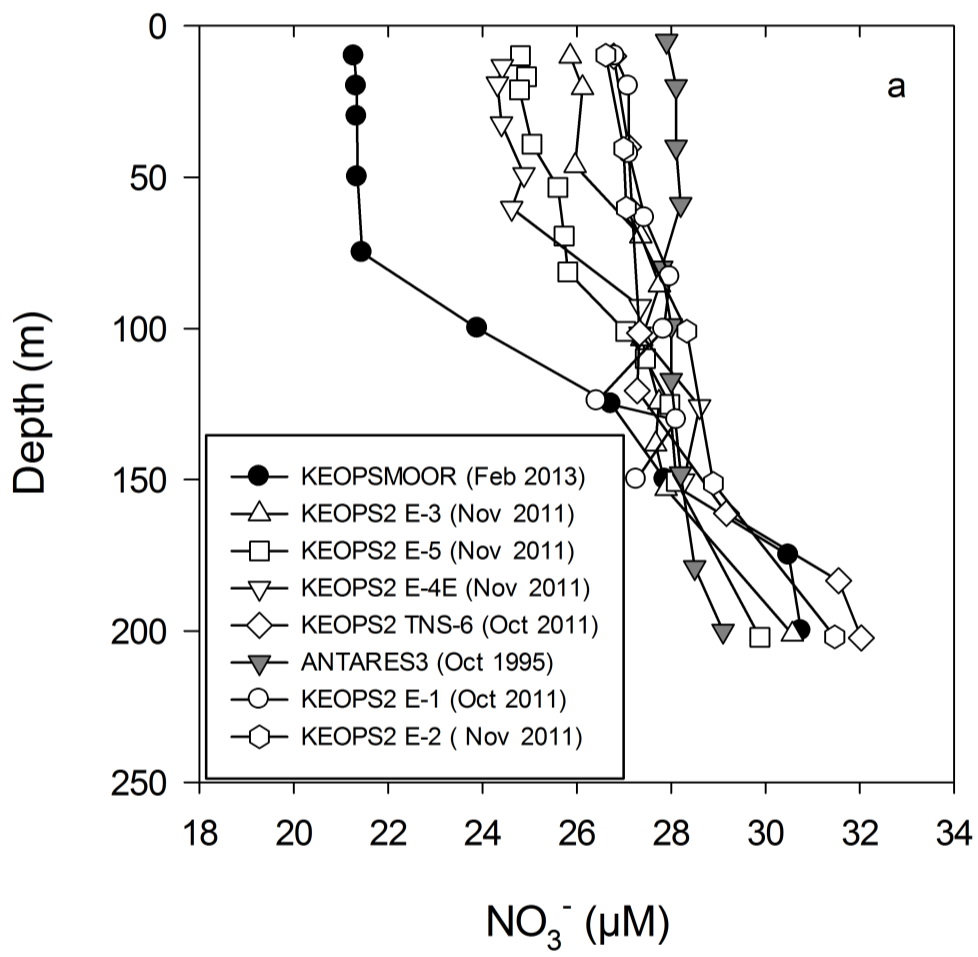


Figure 7

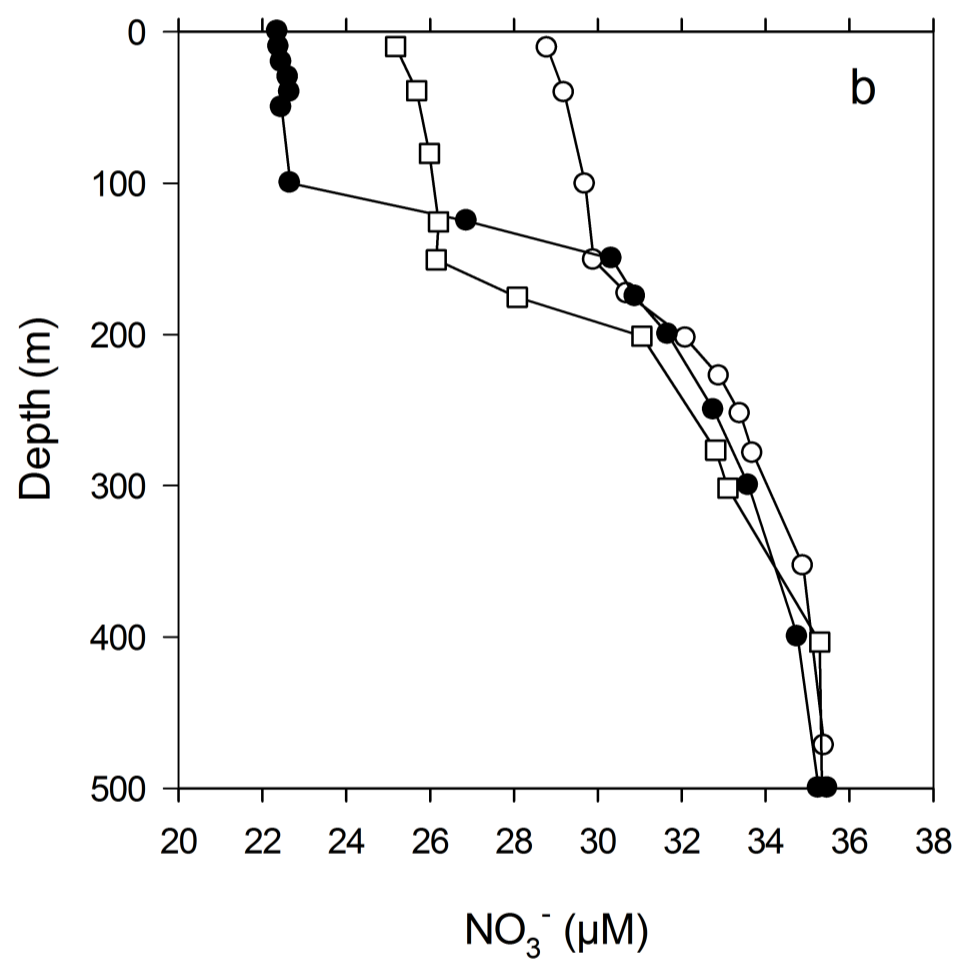
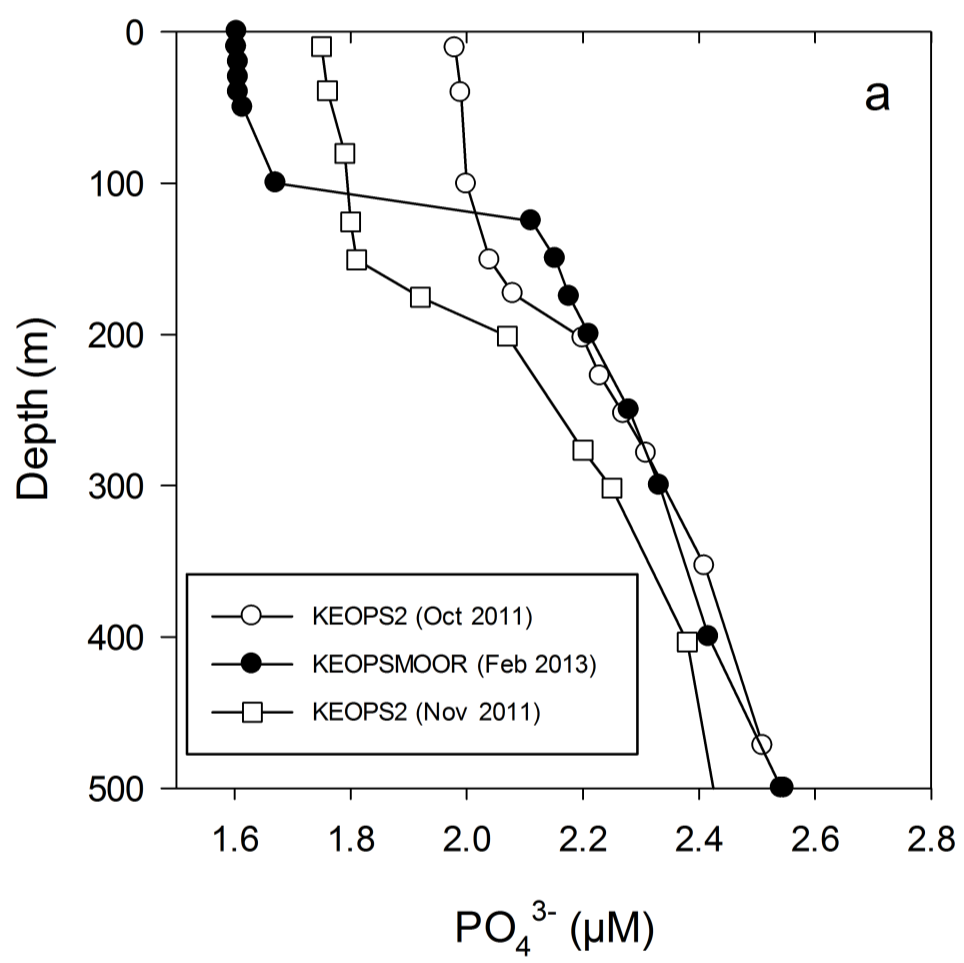


Figure 8

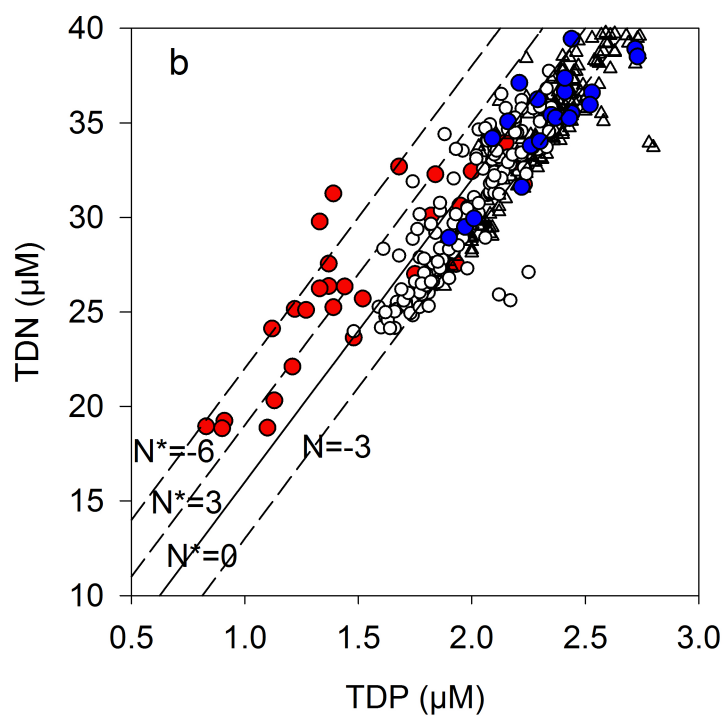
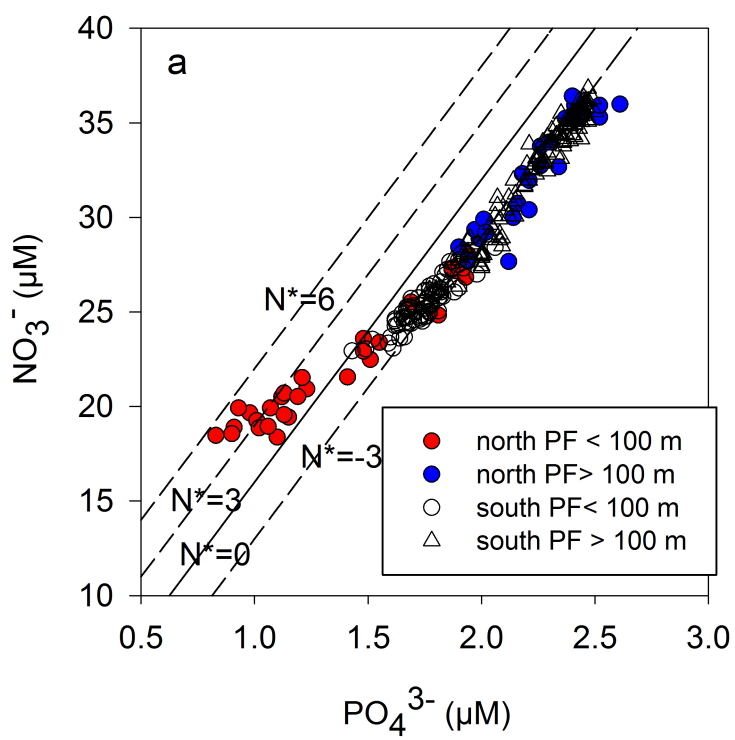


Figure 9

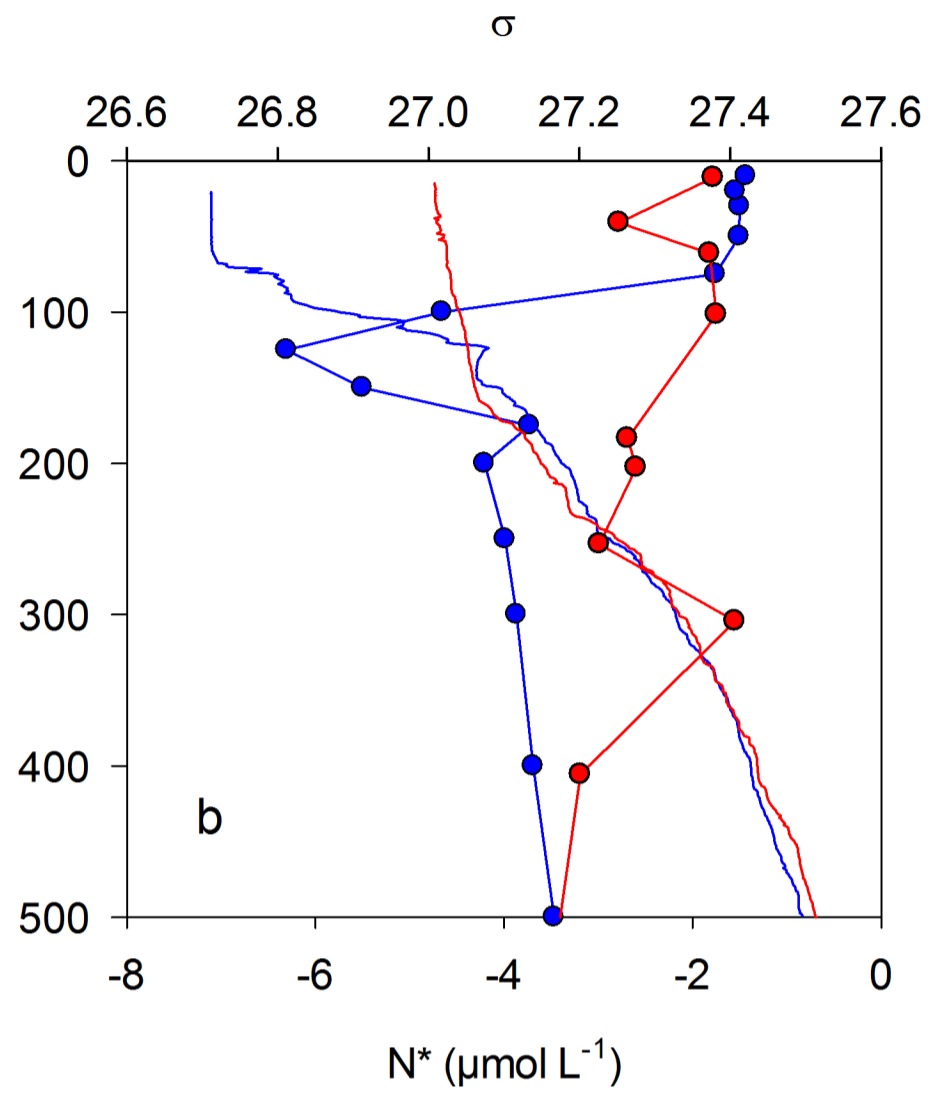
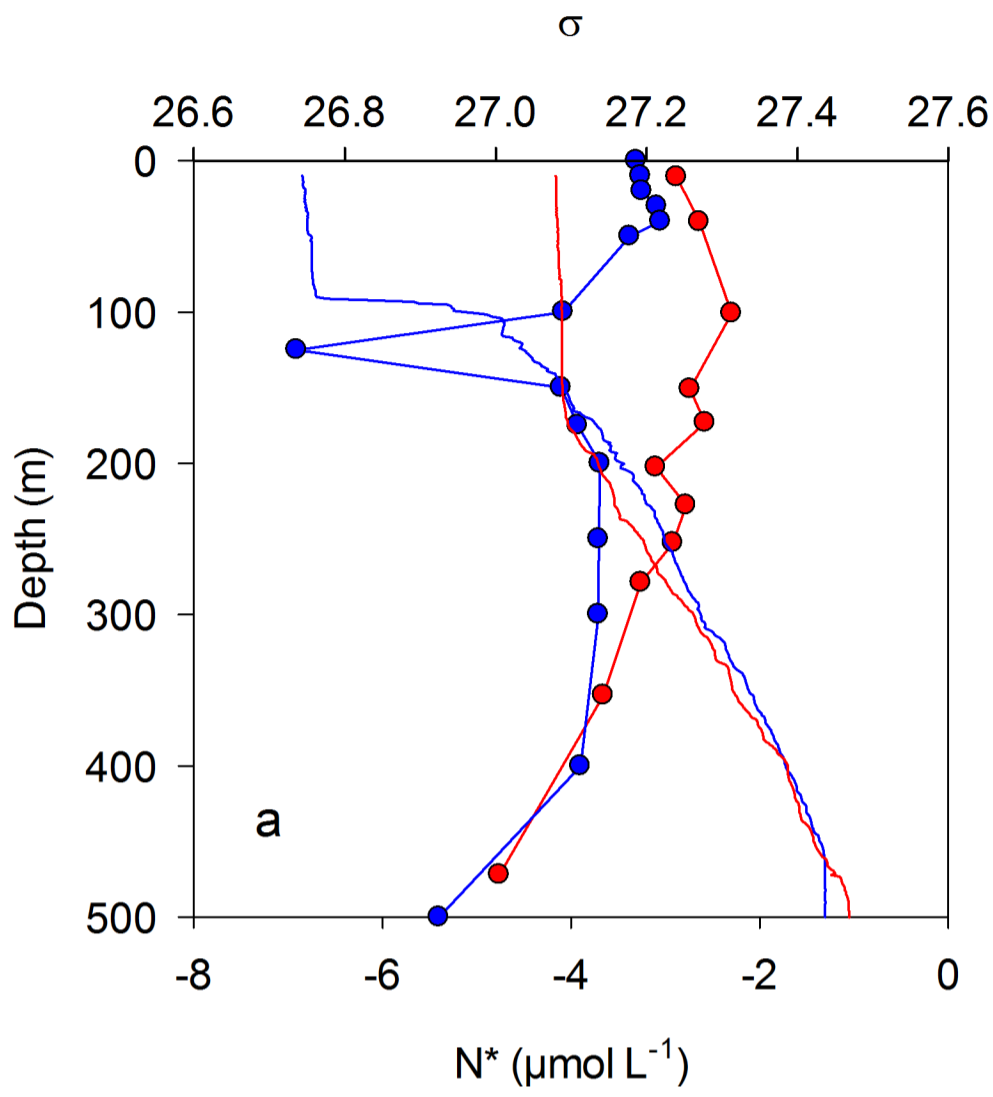


Figure 10